Structural basis for the *O*-acetyltransferase function of the extracytoplasmic domain of OatA from *Staphylococcus aureus*

Received for publication, February 18, 2020, and in revised form, April 27, 2020 Published, Papers in Press, April 29, 2020, DOI 10.1074/jbc.RA120.013108

Carys S. Jones[1], **David Sychantha**[1], **P. Lynne Howell**[2,3], **and Anthony J. Clarke**[1,4,*]

From the [1]*Department of Molecular and Cellular Biology, University of Guelph, Guelph, Ontario, Canada, the* [2]*Program in Molecular Medicine, The Hospital for Sick Children, Toronto, Ontario, Canada, the* [3]*Department of Biochemistry, Faculty of Medicine, University of Toronto, Toronto, Ontario, Canada, and the* [4]*Department of Chemistry and Biochemistry, Wilfrid Laurier University, Waterloo, Ontario, Canada*

Edited by Gerald W. Hart

Many bacteria possess enzymes that modify the essential cell-wall polymer peptidoglycan by *O*-acetylation. This modification occurs in numerous Gram-positive pathogens, including methicillin-resistant *Staphylococcus aureus*, a common cause of human infections. *O*-Acetylation of peptidoglycan protects bacteria from the lytic activity of lysozyme, a mammalian innate immune enzyme, and as such is important for bacterial virulence. The *O*-acetylating enzyme in Gram-positive bacteria, *O*-acetyltransferase A (OatA), is a two-domain protein consisting of an N-terminal integral membrane domain and a C-terminal extracytoplasmic domain. Here, we present the X-ray crystal structure at 1.71 Å resolution and the biochemical characterization of the C-terminal domain of *S. aureus* OatA. The structure revealed that this OatA domain adopts an SGNH-hydrolase fold and possesses a canonical catalytic triad. Site-specific replacement of active-site amino acids revealed the presence of a water-coordinating aspartate residue that limits esterase activity. This residue, although conserved in staphyloccocal OatA and most other homologs, is not present in the previously characterized streptococcal OatA. These results provide insights into the mechanism of acetyl transfer in the SGNH/GDSL hydrolase family and highlight important evolutionary differences between homologous OatA enzymes. Furthermore, this study enhances our understanding of PG *O*-acetyltransferases, which could guide the development of novel antibacterial drugs to combat infections with multidrug-resistant bacterial pathogens.

Antimicrobial resistance is one of the leading healthcare burdens of the century and is only predicted to worsen. Current projections predict that antimicrobial resistant infections will overtake cancer as a leading cause of death worldwide by 2050 (1). Among the biggest threats is methicillin-resistant *Staphylococcus aureus*. Individuals infected with methicillin-resistant *S. aureus* are estimated to be 64% more likely to die than those infected with non–drug-resistant strains of *S. aureus*. Both the Centers for Disease Control and Prevention and the World Health Organization have highlighted the desperate need for the research and development of novel antimicrobials to combat multidrug-resistant infections (2, 3). One approach researchers are taking is to search for ways to disarm bacteria with nontraditional therapeutic agents (4). By targeting virulence factors that significantly contribute to the ability of a bacterium to colonize a host or cause infection, it will be possible to prevent infection without otherwise affecting survivability of the bacterium. It is thought that drugs targeting virulence factors may suffer less from the development of resistance (4).

The peptidoglycan (PG) layer of Gram-negative and Gram-positive bacteria is an essential component of the cell envelope involved in shape determination and resisting turgor pressure. PG is composed of a glycan backbone consisting of alternating *N*-acetylglucosamine (GlcNAc) and *N*-acetylmuramic acid (MurNAc) residues. Glycan chains are cross-linked by short peptides attached to MurNAc residues to form a mesh-like sacculus surrounding the cytoplasmic membrane. The importance of this macromolecule is highlighted by the number of antimicrobials that target PG and steps in its biosynthesis pathway.

Lysozyme is a muramidase of the innate immune system that hydrolyzes the β-1,4-glycosidic bond between MurNAc and GlcNAc residues, causing bacterial cell lysis. Because of the unique nature of PG, released fragments serve as important recognition motifs for immune receptors, activating the immune response in the early stages of an infection (5). Many pathogens have therefore evolved a strategy to defend against the host immune system through modification to their PG.

One such modification is *O*-acetylation of the C6-hydroxyl of MurNAc residues of PG, which sterically hinders binding of lysozyme (6, 7). This modification is widespread among Gram-negative and Gram-positive bacteria, but it is most predominant in pathogens (8–11). Bera *et al.* (12) discovered that only pathogenic species of *Staphylococcus* produce *O*-acetylated PG, and they are resistant to lysozyme. The levels of PG *O*-acetylation can range from 20 to 80% depending on the organism, environmental conditions, and growth phase of the culture (13–15). For example, the levels of PG *O*-acetylation increase by 10–40% as *Enterococcus faecalis* cells enter stationary the phase and a further 10–16% as the cells enter the viable but nonculturable state (16). In addition to providing resistance to lysozyme, PG *O*-acetylation has important implications in virulence, including increasing disease severity and downstream complications (17, 18), conferring resistance to bacteriocins

This article contains supporting information.

* For correspondence: Anthony J. Clarke, ajclarke@wlu.ca.

Present address for David Sychantha: David Braley Centre for Antibiotic Discovery, Michael G. DeGroote Institute for Infectious Disease Research, Dept. of Biochemistry and Biomedical Science, McMaster University, Hamilton, Ontario, Canada.

Table 1
Specific activities of *Sa*OatA$_C$ variants
± denotes standard deviation; ND, no detectable activity.

Enzyme variant	Esterase activity[a]		Transferase activity[b]		T_m[c]
	Specific activity	Relative activity	Specific activity	Relative activity	
	nmol min^{-1} mg^{-1}	*%*	*nmol min^{-1} mg^{-1}*	*%*	*°C*
*Sa*OatA$_C$ (WT)	6.78 ± 0.13	100			
K464A/K465A	7.18 ± 0.090	106			
K495A/K496A	7.70 ± 0.042	114			57.35 ± 0.163
E551A/K552A	7.83 ± 0.057	115			
*Sa*OatA$_C$ (WT)	4.88 ± 0.15	100	0.49 ± 0.19	100	59.49 ± 0.025
S453A	ND	0			54.83 ± 0.233
H578A	0.120 ± 0.0034	2.08			56.96 ± 0.086
D575A	0.060 ± 0.0033	1.06			51.30 ± 0.234
N507A	ND	0			51.26 ± 0.053
V475G	ND	0			51.32 ± 0.057
D457A	18.5 ± 0.20	392	4.25 ± 0.73	866	57.77 ± 0.310
D457N	18.1 ± 0.18	385	3.25 ± 0.80	662	57.59 ± 0.376

[a] The reactions were conducted in 50 mM sodium phosphate at pH 7.0 for the first four variants and pH 6.5 for all others at 25 °C with 0.1 mM 4MU-Ac.
[b] The reactions were conducted in 50 mM sodium phosphate at pH 7.0 at 37 °C with 0.1 mM 4MU-Ac and 2 mM pentaacetyl-chitopentaose
[c] The T_m values were determined for purified *Sa*OatA$_C$ using the thermal shift assay with SYPRO Orange.

(19) and β-lactam antibiotics (10), and influencing the immune response (19, 20). PG *O*-acetylation is considered important for virulence in numerous pathogens such as *S. aureus* (8, 17, 20), *Streptococcus pneumoniae* (10), *Listeria monocytogenes* (19), *Neisseria meningitidis* (21), *Neisseria gonorrhoeae* (9, 18), *Helicobacter pylori* (22), and *E. faecalis* (23).

In Gram-positive bacteria, the enzyme responsible for PG *O*-acetylation is *O*-acetyltransferase A (OatA), first identified in *S. aureus* (8). Homologs of OatA have since been identified in *S. pneumoniae* (10), *L. monocytogenes* (19), *E. faecalis* (23), *Lactobacillus plantarum* (24), *Lactococcus lactis* (25), and several other *Staphylococcus* species (12). OatA is a bimodular protein consisting of an N-terminal acyltransferase 3 integral membrane domain and an extracellular C-terminal SGNH/GDSL-hydrolase domain. SGNH hydrolases are a large family of esterases and lipases that possess four consensus residues, Ser, Gly, Asn, and His, that comprise their active sites and are involved in their mechanism of action (26). The catalytic Ser of these enzymes is found in a GDSL sequence motif. The N-terminal domain of OatA is predicted to contain 11 transmembrane helices and is thought to shuttle acetyl groups across the cytoplasmic membrane to the C-terminal domain for their subsequent transfer onto PG (27). It is still unknown whether the two domains remain attached after translation; *S. aureus* OatA possesses a noncanonical signal peptidase site between the two domains, and the C-terminal domain alone has been detected in spent culture media (28).

We recently described the crystal structure of the C-terminal domain of OatA from *S. pneumoniae* and experimentally confirmed the function of this domain as an *O*-acetyltransferase with a reaction mechanism involving a Ser-His-Asp catalytic triad (29, 30). Preliminary characterization of the C-terminal domain of *S. aureus* OatA was also performed, including identification of the putative catalytic triad residues. Furthermore, the substrate specificity of the C-terminal domains of *S. pneumoniae* and *S. aureus* OatA was investigated with regard to the stem peptide, and it was found that the enzymes had distinct preferences for muroglycans with tetra- and pentapeptide stems, respectively (29). Given that PG *O*-acetylation is a post-biosynthetic modification, occurring after incorporation of lipid II precursors into the pre-existing sacculus (31–34), OatA must work intimately with the PG biosynthetic machinery. Here, we present the crystal structure of the C-terminal domain of *S. aureus* OatA and characterization of its mechanism of action as an *O*-acetyltransferase. Examination of the active center suggests that the staphylococcal enzyme, as well as those produced by most other Gram-positive pathogens, use a novel process for preventing simple hydrolysis of the acetyl-enzyme intermediate compared with the previously characterized streptococcal OatA.

Results

Crystallization and structure determination of Sa*OatA$_C$*

Efforts to crystallize the engineered extracytoplasmic domain of *S. aureus* OatA, encompassing residues 445–601 (*Sa*OatA$_C$), were unsuccessful, despite the removal of potentially disordered regions that could hinder crystallization. This included significant truncation of the N-terminal interdomain-linker regions and two C-terminal lysine residues. To find additional areas of disorder, we analyzed the amino acid sequence of *Sa*OatA$_C$ and found that it was enriched with residues of high conformational freedom (9.6% Lys and 5.1% Glu). Therefore, we used surface entropy reduction (35) in an effort to reduce surface disorder and promote crystallization of the domain. We identified three clusters of predicted high entropy surface residues: Lys^{464} and Lys^{465}, Lys^{495} and Lys^{496}, and Glu^{551} and Lys^{552}, using the SERp server. Each residue in these cluster pairs was replaced with alanine residues to produce three new constructs for crystallization. The specific activities of the resultant *Sa*OatA$_C$ variants were similar to WT enzyme (Table 1), and all three variants crystallized.

(E551A/K552A)-*Sa*OatA$_C$ crystallized only in the presence of zinc salts, so we suspected that Zn^{2+} ions were bound to the protein and well-ordered. Indeed, we detected an anomalous signal from protein-bound zinc, and this signal was sufficient for phase determination using single-wavelength anomalous dispersion (Zn-SAD) (Table 2). (E551A/K552A)-*Sa*OatA$_C$ crystallized with a dimer in the asymmetric unit and contained three Zn^{2+}ions, two of which are coordinated by the putative catalytic His and Asp residues at the dimer interface. We presume that these protein-bound Zn^{2+} ions are not biochemi-

Table 2
Summary of data collection and refinement statistics

	(K495A/K496A)-*Sa*OatA$_C$	(E551A/K552A)-*Sa*OatA$_C$
Data collection		
Beamline	NSLS-II 17-ID2	CLS 08B1-1
Wavelength (Å)	0.99961	1.28167
Space group	$P\,2_1$	$P\,2_1\,2_1\,2_1$
Unit cell parameters		
a (Å)	42.35	39.51
b (Å)	61.30	78.86
c (Å)	67.69	106.59
α (°)	90.00	90.00
γ (°)	90.00	90.00
β (°)	100.90	90.00
Resolution range (last shell) (Å)	28.78–1.71 (1.77–1.71)	44.16–1.55 (1.61–1.55)
Total no. reflections (last shell)	71,747 (6748)	574,457 (19,959)
No. unique reflections (last shell)	36,587 (3545)	46,179 (2983)
Redundancy (last shell)	1.96 (1.90)	12.43 (6.69
Completeness (last shell) (%)	99.36 (96.12)	93.85 (68.8)
Average $I/\sigma I$ (last shell)	17.32 (1.97)	17.53 (4.11)
R_{merge} (last shell, %)[a]	0.02392 (0.4006)	0.09615 (0.3412)
$CC_{½}$ (last shell)[b]	0.999 (0.633)	0.997 (0.97)
Refinement		
R_{work}/R_{free}[c]	0.166/0.196	0.1720/0.1923
No. atoms	2693	2840
Protein	2423	2450
Water	268	389
Ligand	2	3
Average *B*-factor (Å)	31.84	24.82
Protein	30.74	23.41
Water	41.88	33.73
Ligand	26.85	18.46
Root mean square	0.007	0.005
Bond lengths (Å)		
Bond angles (°)	0.82	0.73
Ramachandran total (%)	99.01	98.04
Favored		
Allowed	0.99	1.96
PDB entry	6VJP	6WN9

[a] $R_{merge} = \Sigma_{hkl}\Sigma_i|(I_i(hkl) - <I(hkl)>|/\Sigma_{hkl}\Sigma_i I_i(hkl)$, where *I* is the intensity of the reflection *hkl*, Σ_{hkl} is the sum over all reflections, and Σ_i is the sum over *i* measurements of reflection *hkl*. $<I(hkl)>$ is the mean value of $I(hkl)$.
[b] $CC_{½}$ is the Pearson correlation coefficient calculated between two random half data sets. $CC = \Sigma(x - <x>)(y - <y>)/[\Sigma(x - <x>)^2\Sigma(y - <y>)^2]^{½}$.
[c] $R_{work} = \Sigma_{hkl}|F_{obs} - F_{calc}|/\Sigma_{hkl}|F_{obs}|$, where F_{obs} and F_{calc} are the observed and calculated structure factors, respectively. R_{free} was calculated identically except that all reflections belonged to a test set consisting of only 5% of the data, chosen at random.

cally relevant because they appear to distort the active site. This was supported by the observation that zinc, among other first-row transition metal cations, inhibits *Sa*OatA catalysis *in vitro* (36). Diffraction data were therefore collected for a crystal of (K495A/K496A)-*Sa*OatA$_C$ that grew in the absence of zinc, and the structure was solved by molecular replacement using the (E551A/K552A)-*Sa*OatA$_C$ structure as a search model. This structure was determined to 1.71 Å resolution and refined to R_{work}/R_{free} values of 16.6%/19.6% (Table 2).

The overall structure of (K495A/K496A)-*Sa*OatA$_C$ adopts an α/β-hydrolase fold with five parallel β-strands sandwiched between seven α-helices (Fig. 1). The asymmetric unit contains two molecules of the protein; however, size-exclusion chromatography revealed that *Sa*OatA$_C$ is monomeric, and thus the dimeric conformation seen in the crystal is likely not physiologically relevant. A sodium ion was seen in the bend of α-helix 4 and β-strand 5, coordinated by three water molecules and the backbone carbonyl oxygens of Ala^{550}, Arg^{553}, and Val^{556}. The putative catalytic triad Ser-His-Asp residues align within a shallow active site on the surface of the protein. In chain B, the catalytic His^{578} is found in two conformations, facing both toward and away from the active site (occupancies of 0.54 and 0.46, respectively), suggesting that His^{578} is inherently flexible (Fig. S1).

Searching for structural homologs with DALI revealed that *Sa*OatA$_C$ most closely resembles the C-terminal domain of OatA from *S. pneumoniae* (*Sp*OatA$_C$) (PDB code 5UFY) (Fig. 2*A*). The *Sa*OatA$_C$ structure is also homologous to numerous uncharacterized proteins proposed to belong to the SGNH/GDSL hydrolase family. Of the characterized proteins in the PDB database, aside from *Sp*OatA$_C$, *Sa*OatA$_C$ most closely resembles Axe2, an acetylxylan esterase from *Geobacillus stearothermophilus* (PDB code 4JHL), a family 3 carbohydrate esterase from *Clostridium thermocellum* (PDB code 2VPT), and a family 3 carbohydrate esterase from *Talaromyces cellulolyticus* (PDB code 5B5S) (Fig. 2*A*). The most prominent difference between *Sa*OatA$_C$ and its structural homologs is the geometry of the putative catalytic triad. The distances between Nδ1 of His^{578} and Oδ2 of Asp^{575} and between the ϵ2 of His^{578} and Oγ of Ser^{453} are 3.2 and 4.3 Å, respectively, which are significantly longer than in homologs (Fig. 2*B*). However, in the absence of a bound ligand, the crystal structure of *Sa*OatA$_C$ could represent the inactive resting state of the enzyme and not the active conformation. Indeed, the dual conformations of His^{578} seen in chain B of the crystal structure suggests that His^{578} is flexible (Fig. S1), and the active site may undergo conformational changes during catalysis. Such conformational changes have been reported previously for *Sp*OatA$_C$ and the PG esterase Ape1 (29, 37).

*Sa*OatA$_C$ uses a Ser-His-Asp catalytic triad

SGNH hydrolases are characterized by four consensus sequence blocks (I, II, III, and V) containing conserved residues, Ser, Gly, Asn, and His that, as noted above, give this family of enzymes their name (Ser^{454}, Gly^{475}, Asn^{507}, and His^{578} in *Sa*OatA) (26). Most SGNH hydrolases possess a catalytic triad consisting of a Ser from block I and an Asp and His from block V. The putative catalytic triad residues of *Sa*OatA$_C$, Ser^{453}, His^{578}, and Asp^{575} were previously replaced with Ala in a longer construct of the enzyme (*Sa*OatA$_{435-603}$) and assayed for activity using *p*-nitrophenyl-acetate (*p*NP-Ac) (29). We repeated these experiments using the new construct with 4-methylumbelliferyl-acetate (4MU-Ac) as substrate. The stability of all *Sa*OatA$_C$ variants was verified by a thermal shift assay after purification. The (S453A)-*Sa*OatA$_C$ variant had no detectable activity, whereas the (H578A)-*Sa*OatA$_C$ and (D575A)-*Sa*OatA$_C$ variants had 2.08% and 1.02% residual esterase activity, respectively (Table 1). As seen previously, WT *Sa*OatA$_C$ displays very limited transferase activity toward chito-oligosaccharides as acceptors (29), and as such, it was not possible to determine the rates of transfer for all *Sa*OatA$_C$ variants. A qualitative analysis of any reaction products by LC-MS demonstrated that the truncated WT *Sa*OatA$_C$ retained transferase activity; however, the sensitivity of the assay is not sufficient to discriminate between no transfer and limited transfer that may be seen with weakly active *Sa*OatA$_C$ variants (Fig. S2).

Most SGNH hydrolases employ a double-displacement reaction mechanism involving a covalent acyl-enzyme intermediate at the catalytic serine residue. Indeed, this reaction mechanism was recently confirmed for *Sp*OatA$_C$ (30). We employed a sim-

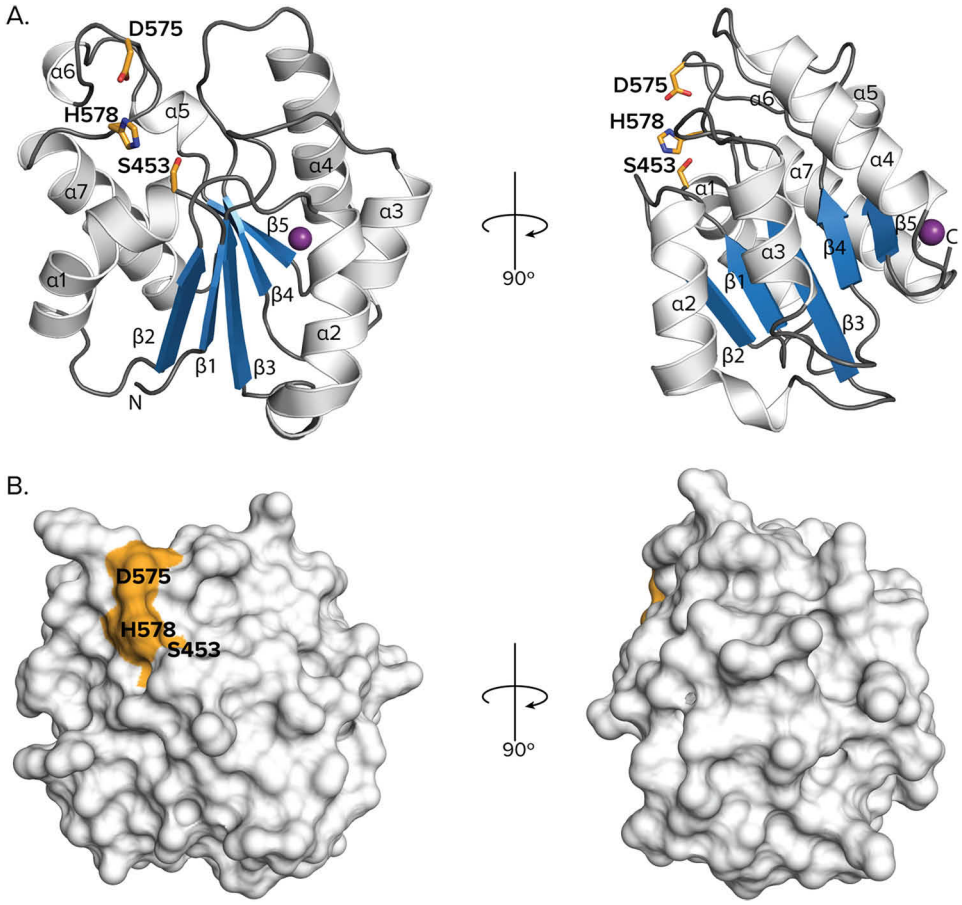

Figure 1. Structure of *Sa*OatA$_C$. *A*, cartoon representation of *Sa*OatA$_C$ showing seven α-helices (*white*) and five β-sheets (*blue*) arranged in an α/β-hydrolase fold. The putative catalytic triad residues are illustrated as *orange sticks*. The sodium atom located between α-helix 4 and β-sheet 5 is indicated by a *purple sphere*. *B*, surface representation of *Sa*OatA$_C$ showing the putative catalytic triad residues in *orange* in a shallow active-site depression.

ilar strategy to unambiguously assign the role of the putative catalytic Ser^{453}. We observed an accumulation of acetyl-*Sa*OatA$_C$ intermediate by real-time analysis of a reaction with *p*NP-Ac as acetyl donor using LC-MS (Fig. 3*A*). *Sa*OatA$_C$ had a molecular mass of 17,562 Da. After incubation with *p*NP-Ac for 15 min, we observed the appearance of multiply charged ions with a decovoluted molecular mass of 17,604 Da. The difference of 42 Da is consistent with the addition of an acetyl group. To identify the acetylated amino acid, we quenched an identical reaction mixture with acetone after 30 min of incubation and digested the recovered enzyme with trypsin. The resulting peptides were separated and analyzed by LC-MS/MS. We observed a pair of peptides, *m*/*z* 1117.59 and 1138.59, with an *m*/*z* difference of 42. The mass and fragmentation patterns of these parent ions correspond well with the native and acetylated forms, respectively, of the peptide ^{442}AASSPLIGD**S**VMVDIGNVFTK^{464} (with Ser^{453} in bold) (Fig. 3*B*). Based on the MS/MS fragmentation pattern of the *m*/*z* 1138.59 parent ion, we were able to map the acetyl modification to Ser^{453}. This *m*/*z* 1138.59 ion was not detected among the digestion products of the no-substrate control reaction.

Sa*OatA$_C$ possesses a typical three-component oxyanion hole*

In most SGNH hydrolases, the oxyanion hole is typically formed by three conserved hydrogen-bond donors: the backbone amide of the catalytic Ser of the block I consensus sequence, the backbone amide of Gly from block II, and the side-chain amide of Asn from block III. In *Sp*OatA$_C$, the block II Gly is replaced by a Ser, and the loop adopts a type I β-turn. In contrast, *Sa*OatA$_C$ retains the Gly, and the loop adopts the typical type II β-turn seen in homologous SGNH esterases (Fig. 2*B*). The backbone amide of Gly^{476} in *Sa*OatA$_C$ faces the active site and thus likely participates in stabilizing the transition state. Interestingly, the Nδ^2 of block III Asn^{507} is only 3.1 Å away from the Oγ of Ser^{453}, closer than typically seen in other SGNH hydrolases. We tested the importance of Asn^{507} in catalysis by its replacement with Ala. The (N507A)-*Sa*OatA$_C$ variant had no detectable esterase activity toward 4MU-Ac, suggesting an important role in the catalytic mechanism (Table 1).

We also previously proposed the importance of a (V/I)(G/S)(R/V) motif in the block II loop (29). In the resting-state structure of *Sp*OatA$_C$, a water molecule was observed coordinated by the backbone carbonyl of Val^{460} and the backbone carbonyl of Val^{462} (equivalent residues Val^{475} and Arg^{477} in *Sa*OatA$_C$) (29). In contrast, because of the opposite turn of the block II loop in *Sa*OatA$_C$, the carbonyl of Val^{475} does not face the active site, and no water molecule is seen coordinated at the active site in this position (Fig. 4 and Fig. S3). Nonetheless, Val^{475} is highly

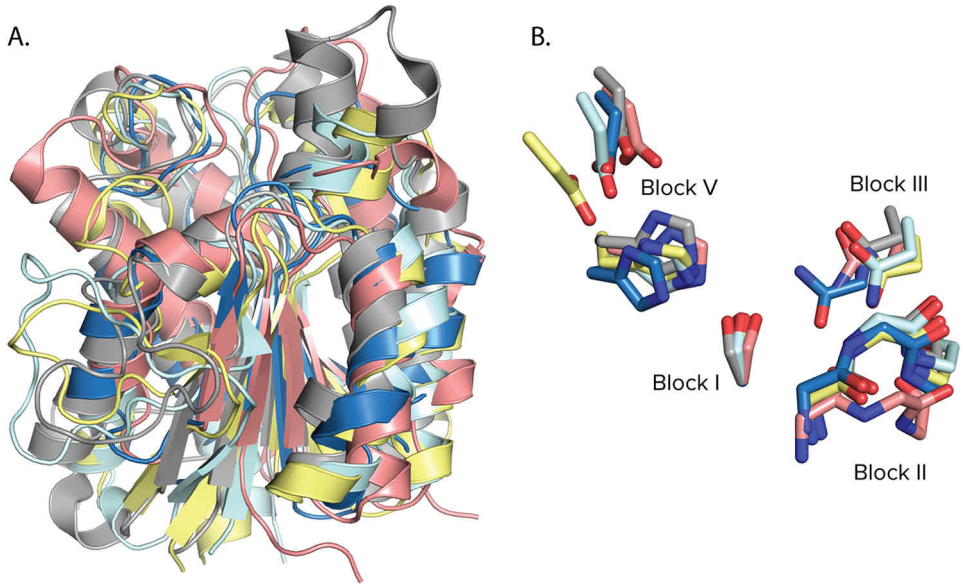

C.

	Block I	Block II	Block III	Block V
*Sa*OatA	LIGDSVMVD	KVGRQL	LGTNG	AYDGIHLE
*Sp*OatA	LIGDSVALR	QVSVTT	TGVND	GTDQVHFG
*Gs*Axe2	FIGDSITDC	ISGNTV	IGIND	AWDRVHPS
*Ct*Ces3	PVGDSCTEG	HSGWTI	IGGND	SWDGLHLS
*Tc*Ces3	LLGDSITEI	HSGWQA	LGTND	RDDGVHPN

Figure 2. Structural comparison of *Sa*OatA$_C$ to SGNH/GDSL hydrolase homologs. *A*, cartoon representation of *Sa*OatA$_C$ (*dark blue*; PDB code 6VJP) overlaid with *Sp*OatA$_C$ (*pink*; PDB code 5UFY), Axe2 from *G. stearothermophilus* (*Gs*Axe2; *gray*; PDB code 4JHL), family 3 carbohydrate esterase from *C. thermocellum* (*Ct*Ces3; *yellow*; PDB code 2VPT), and family 3 carbohydrate esterase from *T. cellulolyticus* (*Tc*Ces3; *pale blue*; PDB code 5B5S). *B*, alignment of the conserved SGNH hydrolase block residues from the aforementioned structural homologs. *C*, block alignments comparing *Sa*OatA, *Sp*OatA, and SGNH hydrolase structural homologs. Catalytic triad and oxyanion hole residues are in *red* and *blue*, respectively, whereas the highly conserved Asp present in most OatA sequences except those of the streptococci node is in *green*. *Sa*OatAC, PDB ID: 6VJP; *Sp*Oat-AC, PDB ID: 5UFY, RMSD: 1.8 Å over 179 equivalent Cα's, z-score: 20, 27% sequence identity; *Gs*Axe2, PDB ID: 4JHL, RMSD: 2.2 Å over 146 equivalent Cα's, z-score: 16.5, 18% sequence identity; *Ct*Ces3, PDB ID: 2VPT, RMSD: 2.2 Å over 147 equivalent Cα's, z-score: 16.7, 14% sequence identity; *Tc*Ces3, PDB ID: 5B5S over 149 equivalent Cα's, RMSD: 2.2 Å, z-score: 16.4, 17% sequence identity.

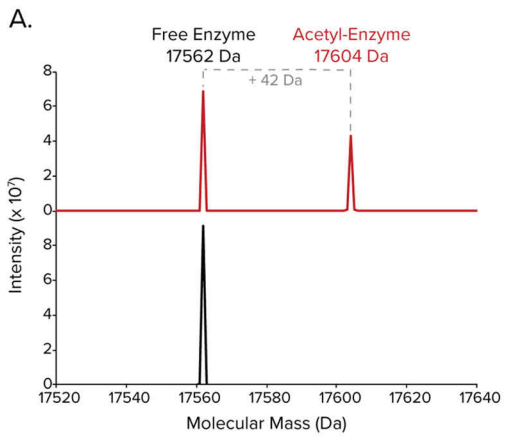

B.

Residue		[M+H]⁺		[M+H]⁺
A	b1	72.044	y22	2276.17
A	b2	143.08	y21	2205.14
S	b3	230.11	y20	2134.10
S	b4	317.14	y19	2047.07
P	b5	414.20	y18	1960.04
L	b6	527.28	y17	1862.98
L	b7	640.37	y16	1749.90
I	b8	753.45	y15	1636.81
G	b9	810.47	y14	1523.73
D	b10	925.50	y13	1466.71
S	b11	1054.53	y12	1351.68
V	b12	1153.60	y11	1222.65
M	b13	1284.64	y10	1123.58
V	b14	1383.71	y9	992.54
D	b15	1498.74	y8	893.47
I	b16	1611.82	y7	778.44
G	b17	1668.84	y6	665.36
N	b18	1782.88	y5	608.34
V	b19	1881.95	y4	494.30
F	b20	2029.02	y3	395.23
T	b21	2130.07	y2	248.16
K	b22	2258.16	y1	147.11

Figure 3. Direct observation of the acetyl-*Sa*OatA$_C$ intermediate. *A*, *Sa*OatA$_C$ was incubated with 1 mM *p*NP-Ac (*red*) or no substrate (*black*) and separated via reverse-phase LC-MS. The resulting mass spectra show the appearance of a peak with a mass increase of 42 Da after incubation with *p*NP-Ac, consistent with the formation of a covalent acetyl-enzyme intermediate. *B*, table showing the expected and observed ions for the fragmentation of an ion from a trypsin-digested reaction of *Sa*OatA$_C$ with *p*NP-Ac. A reaction of *Sa*OatA$_C$ with 1 mM *p*NP-Ac was quenched by the addition of cold acetone. The recovered protein was digested with trypsin, and the resultant peptides were separated by LC-MS/MS. The parent ion had an *m/z* of 1138.7, corresponding to the amino acid sequence shown. The fragmentation pattern was consistent with the acetylation of Ser^{453} (shown in *red*). The observed ions are noted in *green* or *blue*.

conserved among OatA homologs, and in accordance, we replaced Val^{475} with Gly and saw complete abolishment of esterase activity (Table 1).

Conserved Asp^{457} limits esterase activity

We observed a water molecule in the active site of *Sa*OatA$_C$ coordinated by the Oδ1 of Asp^{457}, the backbone carbonyl of

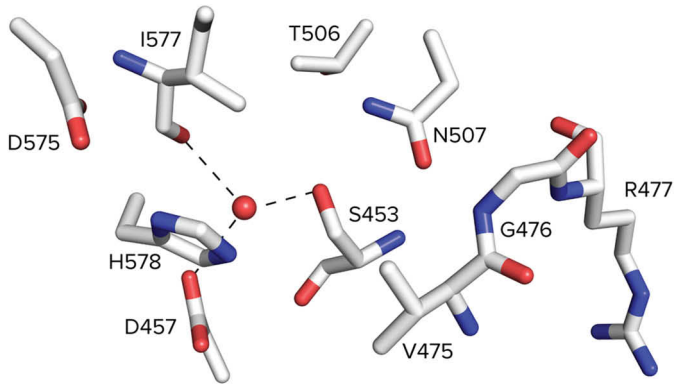

Figure 4. The active site of *Sa*OatA$_C$. A water molecule (*red sphere*) can be seen coordinated by the Oδ1 of Asp^{457}, the backbone carbonyl of Ile^{577}, and the Oγ of the catalytic Ser^{453}.

Ile^{577}, and the Oγ of the catalytic Ser^{453} that was not present in any of the structural esterase homologs or *Sp*OatA$_C$ (Fig. 4). We investigated the role of the water molecule by substituting Asp^{457} with Ala and Asn. Surprisingly, the D457A and D457N variants of *Sa*OatA$_C$ displayed a 4-fold increase in esterase activity and still maintained the ability to transfer to chitooligosaccharides (Table 1). To investigate the prevalence of an Asp at this position in SGNH hydrolases/transferases, we analyzed sequences from 200 known and hypothetical OatA homologs from Gram-positive bacteria and characterized esterases from the SGNH hydrolase family. We found that an Asp is highly conserved in OatA homologs from the *Staphyloccocus*, *Bacillus*, *Listeria*, and *Lactobacillus* genera, among others (Fig. S4). In contrast, an Asp residue was not found at this position (catalytic Ser + 4) in any of the characterized SGNH hydrolases that naturally act as esterases (Fig. 2*C*). In most OatA homologs from *Streptococcus* species, an Arg residue is found in this position (Fig. S4). We propose that Asp^{457} is a conserved feature in many SGNH family transferases and serves as a sentry to limit esterase activity through the coordination of a water molecule that could otherwise approach an acetyl-enzyme intermediate. It was observed that transferase activity also increased with the replacement of Asp^{457} with Ala or Asn. The reason for this enhanced activity is not known, but it is possible that these replacements increase the accessibility of the pseudo-substrate chitooligosaccharides, in addition to water, used as acceptors for the *in vitro* assays of transferase activity.

Discussion

OatA belongs to the SGNH hydrolase family of enzymes along with numerous esterases with a wide range of substrate specificities. The mechanism by which OatA acts as a transferase was widely unknown until recently. The structure of *Sp*OatA$_C$ elucidated structural features that distinguished it from SGNH hydrolase family esterases, including an inverted turn of the block II loop, a conserved valine in block II, a hydrophobic active site wall, and an atypical two-residue oxyanion hole (29). Unexpectedly, the active site of *Sa*OatA$_C$ more closely resembles that of structurally homologous esterases than that of *Sp*OatA$_C$. *Sa*OatA$_C$ has the conserved Gly in block II, and the loop adopts the typical type II β-turn seen in the homologous esterases. As a consequence, the water molecule that is coordinated by the backbone of Val^{460} in the block II sequence of *Sp*OatA$_C$ in its resting state is not seen in the structure of *Sa*OatA$_C$. Furthermore, replacement of Val^{460} of *Sp*OatA$_C$ with Gly or Ala increases esterase activity while resulting in loss of transferase activity (29). To explain this loss, it was proposed that Val^{460} may contribute to the effective binding of the carbohydrate acceptor. In contrast, a comparative replacement of the homologous Val in *Sa*OatA$_C$, Val^{475} resulted in a total loss of esterase activity. It is possible that replacement of Val^{475} with Gly in *Sa*OatA$_C$ disrupts correct positioning of the block II loop, which may impact the ability of the backbone amide of Gly^{476} to stabilize the transition state; such stabilization of the transition state formed by *Sp*OatA$_C$ does not appear to involve its block II loop (29).

A thorough kinetic analysis of *Sp*OatA$_C$ confirmed that the enzyme employs a double-displacement reaction mechanism (30). Accordingly, we propose that *Sa*OatA$_C$ follows a similar reaction mechanism (Fig. S5), wherein the carboxyl group of Asp^{575} forms a salt bridge with a nitrogen atom in the imidazole ring of His^{578}, enabling His^{578} to deprotonate Ser^{453}. The nucleophilic Ser^{453} attacks the carbonyl carbon of the acetyl donor, generating a tetrahedral transition state. Residues at the active center of the enzyme form an oxyanion hole that stabilizes the transition state, which then collapses into a covalently bound acetyl-enzyme intermediate. We were able to unequivocally identify Ser^{453} of *Sa*OatA$_C$ as the site of acetylation (Fig. 3). The acetyl donor is released upon acquisition of a proton from His^{578}. The glycan accepter, a MurNAc residue of the PG backbone, can then bind the active site cleft. His^{578}, now acting as a base, abstracts a proton from the C6-OH of MurNAc, rendering the carbon atom nucleophilic and resulting in its attack on the carbonyl center of the acetyl-Ser^{453} intermediate. This leads to the formation of a second tetrahedral transition state, collapse of which results in the release of the *O*-acetylated product and free enzyme.

We propose that the transition state is stabilized by the backbone amide of Ser^{453} in block I, the side-chain amide of Asn^{507} in block III, and the backbone amide of Gly^{476} in block II. The three-residue oxyanion hole is typical of SGNH hydrolases, but distinguishes *Sa*OatA$_C$ from *Sp*OatA$_C$, which appears to employ an oxyanion hole formed of two residues (29). Replacement of the *Sp*OatA$_C$ block III Asn^{491} with Ala gave 58% residual esterase activity (29). Further kinetic analysis suggested that Asn^{491} may play a larger role in substrate binding than in stabilization of the first transition state (30). In contrast, replacement of Asn^{507} of *Sa*OatA$_C$ with Ala resulted in a complete loss of activity, suggesting that this residue may play a more critical role in *Sa*OatA$_C$. Absolute identification of oxyanion hole H-donors would require analysis of a ligand-bound structure, ideally with a covalently bound transition-state mimic. Such a structure was achieved for *Sp*OatA$_C$ using the mechanistic inhibitor methanesulfonyl fluoride, forming a methylsulfonyl-adduct structure (PDB code 5UG1). Unfortunately, methanesulfonyl fluoride and related analogs do not significantly inhibit *Sa*OatA$_C$; thus a different transition state mimic will need to be found.

Bioinformatic analysis shows that OatA homologs form two distinct clades, wherein the *Streptococcus* genus forms a phylo-

genetically separate clade to *Staphylococcus*, *Bacillus*, and other genera (Fig. S4). The differences that we have observed between the structures of *S. pneumoniae* and *S. aureus* OatA suggest that the enzymes from these clades may use different mechanisms to minimize, if not prevent, water from serving as the acetyl acceptor during their respective double-displacement reaction mechanisms. We previously noted the occurrence of a conserved Val/Ile adjacent to the oxyanion hole block III Asn in *Streptococcus* OatA homologs, proposing that this hydrophobic residue may stabilize carbohydrate acceptor substrates (29). In contrast, in *Staphylococcus* and species from the same clade, this position is most commonly occupied by a Thr or Ser residue, which would not engage in the same hydrophobic interactions. We identified a water molecule coordinated by Asp^{457} in the structure of *Sa*$OatA_C$ and determined that this residue played an important role in limiting the esterase activity of the enzyme, while maintaining transferase activity. This suggests that the two distinct clades of OatA homologs utilize different mechanisms to preclude water from their active site to catalyze efficient and nonwasteful transfer of acetyl groups to peptidoglycan only. Our data suggest that the coordination of a water molecule in the active site by Asp^{457} may be the method by which *Sa*$OatA_C$ and the majority of OatA homologs belonging to the same phylogenetic clade favor transferase activity. Unfortunately, the absence of other OatA structures prevents us from verifying whether or not these structural features are conserved among homologs within the same clade. The reason for these differences also remains unknown. Perhaps the selective pressure for divergence into two clades was substrate specificity recognizing that the staphylococcal OatA O-acetylates MurNAc residues with pentapeptide stems, whereas the streptococcal enzyme has specificity for residues with tetrapeptide stems (29).

PG *O*-acetylation is a common modification employed by pathogenic Gram-positive bacteria as a means to evade the host innate immune system. Despite knowledge of the modification for decades, OatA from *S. pneumoniae* was the only PG *O*-acetylating enzyme from a Gram-positive bacteria characterized before this study. Our data reinforce the mechanism of action proposed for both *S. pneumoniae* $OatA_C$ and *N. gonorrhoeae* peptidoglycan *O*-acetyltransferase B (PatB) (30, 38). We have previously validated *Sa*$OatA_C$ and *N. gonorrhoeae* PatB as antibiotic targets with a high-throughput small-molecule screen (39). The structure of *Sa*$OatA_C$ will assist in the design of anti-virulence drugs against OatA. Furthermore, our discovery of the differences between the active sites of *S. pneumoniae* and *S. aureus* $OatA_C$ is an important consideration in developing narrow- or broad-spectrum OatA inhibitors for the treatment of important human pathogens for which current antibacterial therapies are being threatened by multidrug resistance.

Experimental procedures

Cloning of C-terminal S. aureus *oatA variants*

The generation of *Sa*$OatA_{C(445–601)}$ possessing single site-specific amino acid replacements was achieved by site-directed mutagenesis. PCR products incorporating the desired mutations were obtained using KAPA HiFi polymerase with pDSAC71 (harboring $oatA_C$ encoding residues 445–601 of full-length *S. aureus* OatA) as template and the appropriate primers listed in Table S1. Following PCR amplification, the reaction was incubated with Dpn1 (Thermo Fisher Scientific, Mississauga, Canada) for 1 h at 37 °C, followed by transformation into *Escherichia coli* DH5α. The sequences of all resultant plasmids were verified before use.

Overproduction and purification of Sa$OatA_C$

The genes encoding *Sa*$OatA_{C(445–601)}$ and variants were expressed in *E. coli* BL21 (DE3) transformed with pDSAC71, and the overproduced recombinant proteins were purified by a combination of affinity chromatography and gel filtration as previously described (39). Gel filtration buffer consisting of 50 mM Tris, pH 7.5, 150 mM NaCl was used when the protein was being purified for the purpose of crystallography. In all other instances, the gel filtration buffer consisted of 50 mM sodium phosphate, pH 6.5, 150 mM NaCl. Fresh immobilized metal affinity chromatography resin was used for each *Sa*$OatA_C$ variant to prevent cross-contamination.

The stability of each purified protein was assessed by SYPRO Orange thermal shift assay as a means to infer proper folding (40). Briefly, Sa$OatA_C$ and variants were diluted to 5 μM in 50 mM sodium phosphate, pH 7.0, and mixed with 2× SYPRO Orange (Thermo Fisher Scientific) in 50-μl reactions. The melting temperature (T_m) of each protein was determined using a StepOnePlus real-time PCR machine using a temperature gradient of 4 to 95 °C over 60 min. The data were analyzed using the StepOnePlus software.

Crystallization

Sa$OatA_C$ surface entropy variants were concentrated to 30 mg/ml by ultrafiltration using an Amicon Ultra-15 centrifugal filter (10-kDa molecular mass cutoff; Millipore) (4,000 × *g*, 4 °C). Commercial Midwest Center for Structural Genomics crystallization suite sparse matrix crystallization screens 1–4 (Microlytic North America Inc., Burlington, MA, USA) were prepared at room temperature with the E551A/K552A and K495A/K496A forms of Sa$OatA_C$. Crystallization screening by sitting-drop vapor diffusion was set up using a Gryphon robot (Art Robbins Instruments, Sunnyvale, CA, USA) with 1-μl protein drops and a protein-to-reservoir ratio of 1:1 for a final drop volume of 2 μl. Crystal trays were stored at 22 °C. Optimization of crystal conditions was performed to produce crystals of (E551A/K552A)-Sa$OatA_C$ in 0.008 M zinc acetate, 20% PEG 3350, and crystals of (K495A/K496A)-Sa$OatA_C$ in 27% PEG 6000, 0.015 M sodium citrate.

X-ray diffraction data collection and structure determination

Crystals were cryoprotected for 30 s in reservoir solution supplemented with 60% (v/v) ethylene glycol prior to vitrification in liquid nitrogen. Zn-SAD data for (E551A/K552A)-*Sa*$OatA_C$ were collected on Beamline 08B1-1 at the Canadian Synchrotron Light Source (Saskatoon, Canada). Native data for (K495A/K496A)-*Sa*$OatA_C$ were collected on Beamline 17-ID2 at the National Synchrotron Light Source II (Upton, NY). The

data were indexed and scaled using HKL2000 (41). Three zinc sites were located in the (E551A/K552A)-*Sa*OatA$_C$ Zn-SAD data using HKL2MAP (42), and density modified phases were calculated using SOLVE/RESOLVE (43). The resulting electron density map was of good quality and allowed for PHENIX AutoBuild (44) to build 100% of the protein. Manual model building was done in COOT (45) alternated with refinement using PHENIX.REFINE (46). The structure of native (K495A/K496A)-SaOatA$_C$ was determined by molecular replacement using PHENIX AutoMR (46) with the zinc-incorporated derivative as the search model. Manual model building and refinement was carried out as described previously. All molecular models were generated using PyMOL.

Steady-state kinetics of Sa*OatA*$_C$

The specific activity of *Sa*OatA$_C$ acting as an esterase and transferase was determined as previously described (39). Briefly, *Sa*OatA$_C$ (5 μM) was incubated in 50 mM sodium phosphate, pH 6.5, at room temperature with 0.1 mM 4MU-Ac as substrate. For transferase assays, *Sa*OatA$_C$ (5 μM) was incubated in 50 mM sodium phosphate, pH 6.5, at 37 °C with 0.1 mM 4MU-Ac as acetyl donor and 2 mM pentaacetyl-chitopentaose (Megazyme) as acetyl acceptor. Product release was monitored fluorometrically using a Synergy plate reader with excitation and emission wavelengths of 325 and 450 nm, respectively. Control reactions were performed using gel-filtration buffer in place of *Sa*OatA$_C$ to account for spontaneous substrate hydrolysis. The rate of background hydrolysis was subtracted from the rate of reactions with enzyme to determine a rate of esterase activity. The rate of transfer was determined as the difference between the reaction rates with and without acceptor. Each reaction was performed in triplicate. Analyses and graphs were generated in GraphPad Prism 5.

Qualitative analysis of Sa*OatA*$_C$ *transferase activity*

The ability of *Sa*OatA$_C$ to transfer acetyl groups to chitooligosaccharides was determined by qualitative end-point analysis by LC-MS/MS. *Sa*OatA$_C$ (5 μM) was incubated with 0.1 mM 4MU-Ac and 1 mM pentaacetyl-chitopentaose (Megazyme) at 37 °C for 18 h. The reaction products were separated by LC-MS/MS using an Agilent 1200 HPLC system interfaced with an Agilent UHD 6520 Q-TOF mass spectrometer (Agilent Technologies Inc., Santa Clara, CA, USA) housed in the Mass Spectrometry Facility of the Advanced Analysis Centre of the University of Guelph. Data analysis was performed using Mass-Hunter qualitative analysis, version B.06.00 (Agilent).

*Trapping acetyl-*Sa*OatA*$_C$ *intermediate*

Direct observation of the covalent acetyl-SaOatA$_C$ intermediate was achieved by real-time analysis of a reaction by LC-MS as previously described (30) with minor modifications. The reaction mixture consisted of 5 μM *Sa*OatA$_C$ in 50 mM sodium phosphate, pH 6.5, with 1 mM *p*NP-Ac as acetyl donor and was incubated for 15 min in an MS-grade sample vial. A control reaction without *p*NP-Ac was also performed. The site of *O*-acetylation was identified by a tryptic digest of an acetone-quenched reaction mixture of SaOatA$_C$ with *p*NP-Ac, as previously described (30). In this case, the reaction mixture consisted of 5 μM *Sa*OatA$_C$ in 50 mM sodium phosphate, pH 6.5, with 1 mM *p*NP-Ac, incubated for 30 min in an MS-grade sample vial. A control reaction without *p*NP-Ac was also performed. All samples and experiments were run as previously described (30). Data analyses were performed using MassHunter qualitative analysis, version B.06.00 (Agilent).

Other analytical procedures

Nucleotide sequencing of PCR products and plasmids was performed by the Genomics Facility of the Advanced Analysis Center (University of Guelph). Protein concentrations were determined using the Pierce BCA protein assay kit with BSA serving as the standard. SDS-PAGE on 15% acrylamide gels was conducted by the method of Laemmli (47) with Coomassie Brilliant Blue staining. Surface entropy reduction analyses were conducted using the SERp server (35).

Data availability

The atomic coordinates and structure factors of the reported crystal structures have been deposited in the Protein Data Bank under codes 6VJP and 6WN9. The authors declare that all other data supporting the findings of this study are available within the paper and its supporting information.

Acknowledgments—We thank Bryan Fraser for excellent assistance with the production and purification of some of the OatA$_C$ variants and Dr. Natalie Bamford for X-ray diffraction data collection. The Life Science Biomedical Technology Research resource at National Synchrotron Light Source II is primarily supported by the NIGMS, National Institute of Health through Biomedical Technology Research Resource P41 Grant P41GM111244 and by Department of Energy Office of Biological and Environmental Research Grant KP1605010. Beamline 08B1-1 at the Canadian Light Source is supported by the Natural Sciences and Engineering Research Council of Canada, the Canadian Institutes of Health Research, the National Research Council of Canada, the Province of Saskatchewan, Western Economic Diversification Canada, and the University of Saskatchewan.

Author contributions—C. S. J., D. S., and A. J. C. conceptualization; C. S. J. and A. J. C. data curation; C. S. J. and A. J. C. formal analysis; C. S. J., D. S., and P. L. H. validation; C. S. J. investigation; C. S. J. and A. J. C. methodology; C. S. J. writing-original draft; C. S. J., D. S., P. L. H., and A. J. C. writing-review and editing; A. J. C. resources; A. J. C. supervision; A. J. C. funding acquisition; A. J. C. project administration.

Funding and additional information—This work was supported by Canadian Institutes of Health Research Operating Grant PJT156353 (to A. J. C.); an operating grant from the Canadian Glycomics Network, a National Centre of Excellence (to A. J. C.); postgraduate scholarships from the Natural Sciences and Engineering Research Council and the Province of Ontario (to C. S. J.); and a Canadian Research Chair (to P. L. H.).

Conflict of interest—The authors declare that they have no conflicts of interest with the contents of this article.

Abbreviations—The abbreviations used are: PG, peptidoglycan; MurNAc, *N*-acetylmuramic acid; OatA, *O*-acetyltransferase A; Zn-

SAD, zinc single-wavelength anomalous dispersion; *p*NP-Ac, *p*-nitrophenyl-acetate; 4MU-Ac, 4-methylumbelliferyl-acetate; PDB, Protein Data Bank.

References

1. Review on Antimicrobial Resistance (2014) *Antimicrobial Resistance: Tackling a Crisis for the Health and Wealth of Nations*. amr-review.org, London, UK
2. World Health Organization (2017) *Global Priority List of Antibiotic-resistant Bacteria to Guide Research, Discovery, and Development of New Antibiotics*. WHO, Geneva, Switzerland
3. Centers for Disease Control and Prevention (2013) *Antibiotic Resistance Threats in the United States*. U.S. Department of Health and Human Services, CDC, Atlanta, GA
4. Rex, J. H., Fernandez Lynch, H., Cohen, I. G., Darrow, J. J., and Outterson, K. (2019) Non-traditional antibacterial agents. *Nat. Commun.* **10,** 3416 CrossRef Medline
5. Sorbara, M. T., and Philpott, D. J. (2011) Peptidoglycan: a critical activator of the mammalian immune system during infection and homeostasis. *Immunol. Rev.* **243,** 40–60 CrossRef Medline
6. Pushkaran, A. C., Nataraj, N., Nair, N., Götz, F., Biswas, R., and Mohan, C. G. (2015) Understanding the structure-function relationship of lysozyme resistance in *Staphylococcus aureus* by peptidoglycan *O*-acetylation using molecular docking, dynamics, and lysis assay. *J. Chem. Inf. Model.* **55,** 760–770 CrossRef Medline
7. Dupont, C., and Clarke, A. J. (1991) Dependence of lysozyme-catalysed solubilization of *Proteus mirabilis* peptidoglycan on the extent of *O*-acetylation. *Eur. J. Biochem.* **195,** 763–769 CrossRef Medline
8. Bera, A., Herbert, S., Jakob, A., Vollmer, W., and Götz, F. (2005) Why are pathogenic staphylococci so lysozyme resistant?: The peptidoglycan *O*-acetyltransferase OatA is the major determinant for lysozyme resistance of *Staphylococcus aureus*. *Mol. Microbiol.* **55,** 778–787 Medline
9. Blundell, J. K., Smith, G. J., and Perkins, H. R. (1980) The peptidoglycan of *Neisseria gonorrhoeae*: *O*-acetyl groups and lysozyme sensitivity. *FEMS Microbiol. Lett.* **9,** 259–261 CrossRef
10. Crisóstomo, M. I., Vollmer, W., Kharat, A. S., Inhülsen, S., Gehre, F., Buckenmaier, S., and Tomasz, A. (2006) Attenuation of penicillin resistance in a peptidoglycan *O*-acetyl transferase mutant of *Streptococcus pneumoniae*. *Mol. Microbiol.* **61,** 1497–1509 CrossRef Medline
11. Laaberki, M.-H., Pfeffer, J., Clarke, A. J., and Dworkin, J. (2011) *O*-Acetylation of peptidoglycan is required for proper cell separation and S-layer anchoring in *Bacillus anthracis*. *J. Biol. Chem.* **286,** 5278–5288 CrossRef Medline
12. Bera, A., Biswas, R., Herbert, S., and Götz, F. (2006) The presence of peptidoglycan *O*-acetyltransferase in various staphylococcal species correlates with lysozyme resistance and pathogenicity. *Infect. Immun.* **74,** 4598–4604 CrossRef Medline
13. Clarke, A. J. (1993) Extent of peptidoglycan *O*-acetylation in the tribe *Proteeae*. *J. Bacteriol.* **175,** 4550–4553 CrossRef Medline
14. Johannsen, L., Labischinski, H., Reinicke, B., and Giesbrecht, P. (1983) Changes in the chemical structure of walls of *Staphylococcus aureus* grown in the presence of chloramphenicol. *FEMS Microbiol. Lett.* **16,** 313–316 CrossRef
15. Swim, S. C., Gfell, M. A., Wilde, C. E., 3rd, and Rosenthal, R. S. (1983) Strain distribution in extents of lysozyme resistance and *O*-acetylation of gonococcal peptidoglycan determined by high-performance liquid chromatography. *Infect. Immun.* **42,** 446–452 CrossRef Medline
16. Pfeffer, J. M., Strating, H., Weadge, J. T., and Clarke, A. J. (2006) Peptidoglycan *O*-acetylation and autolysin profile of *Enterococcus faecalis* in the viable but nonculturable state. *J. Bacteriol.* **188,** 902–908 CrossRef Medline
17. Baranwal, G., Mohammad, M., Jarneborn, A., Reddy, B. R., Golla, A., Chakravarty, S., Biswas, L., Götz, F., Shankarappa, S., Jin, T., and Biswas, R. (2017) Impact of cell wall peptidoglycan *O*-acetylation on the pathogenesis of *Staphylococcus aureus* in septic arthritis. *Int. J. Med. Microbiol.* **307,** 388–397 CrossRef Medline
18. Fleming, T. J., Wallsmith, D. E., and Rosenthal, R. S. (1986) Arthropathic properties of gonococcal peptidoglycan fragments: implications for the pathogenesis of disseminated gonococcal disease. *Infect. Immun.* **52,** 600–608 CrossRef Medline
19. Aubry, C., Goulard, C., Nahori, M. A., Cayet, N., Decalf, J., Sachse, M., Boneca, I. G., Cossart, P., and Dussurget, O. (2011) OatA, a peptidoglycan *O*-acetyltransferase involved in *Listeria monocytogenes* immune escape, is critical for virulence. *J. Infect. Dis.* **204,** 731–740 CrossRef Medline
20. Sanchez, M., Kolar, S. L., Müller, S., Reyes, C. N., Wolf, A. J., Ogawa, C., Singhania, R., De Carvalho, D. D., Arditi, M., Underhill, D. M., Martins, G. A., and Liu, G. Y. (2017) *O*-Acetylation of peptidoglycan limits helper T cell priming and permits *Staphylococcus aureus* reinfection. *Cell Host Microbe* **22,** 543–551.e4 CrossRef Medline
21. Veyrier, F. J., Williams, A. H., Mesnage, S., Schmitt, C., Taha, M. K., and Boneca, I. G. (2013) De-*O*-acetylation of peptidoglycan regulates glycan chain extension and affects *in vivo* survival of *Neisseria meningitidis*. *Mol. Microbiol.* **87,** 1100–1112 CrossRef Medline
22. Wang, G., Lo, L. F., Forsberg, L. S., and Maier, R. J. (2012) *Helicobacter pylori* peptidoglycan modifications confer lysozyme resistance and contribute to survival in the host. *MBio.* **3,** e00409-12 Medline
23. Hébert, L., Courtin, P., Torelli, R., Sanguinetti, M., Chapot-Chartier, M.-P., Auffray, Y., and Benachour, A. (2007) *Enterococcus faecalis* constitutes an unusual bacterial model in lysozyme resistance. *Infect. Immun.* **75,** 5390–5398 CrossRef Medline
24. Bernard, E., Rolain, T., David, B., André, G., Dupres, V., Dufrêne, Y. F., Hallet, B., Chapot-Chartier, M. P., and Hols, P. (2012) Dual role for the *O*-acetyltransferase OatA in peptidoglycan modification and control of cell septation in *Lactobacillus plantarum*. *PLoS One* **7,** e47893 CrossRef Medline
25. Veiga, P., Bulbarela-Sampieri, C., Furlan, S., Maisons, A., Chapot-Chartier, M.-P., Erkelenz, M., Mervelet, P., Noirot, P., Frees, D., Kuipers, O. P., Kok, J., Gruss, A., Buist, G., and Kulakauskas, S. (2007) SpxB regulates *O*-acetylation-dependent resistance of *Lactococcus lactis* peptidoglycan to hydrolysis. *J. Biol. Chem.* **282,** 19342–19354 CrossRef Medline
26. Akoh, C. C., Lee, G. C., Liaw, Y. C., Huang, T. H., and Shaw, J. F. (2004) GDSL family of serine esterases/lipases. *Prog. Lipid Res.* **43,** 534–552 CrossRef Medline
27. Moynihan, P. J., and Clarke, A. J. (2011) *O*-Acetylated peptidoglycan: controlling the activity of bacterial autolysins and lytic enzymes of innate immune systems. *Int. J. Biochem. Cell Biol.* **43,** 1655–1659 CrossRef Medline
28. Schallenberger, M. A., Niessen, S., Shao, C., Fowler, B. J., and Romesberg, F. E. (2012) Type I signal peptidase and protein secretion in *Staphylococcus aureus*. *J. Bacteriol.* **194,** 2677–2686 Medline
29. Sychantha, D., Jones, C. S., Little, D. J., Moynihan, P. J., Robinson, H., Galley, N. F., Roper, D. I., Dowson, C. G., Howell, P. L., and Clarke, A. J. (2017) *In vitro* characterization of the antivirulence target of Gram-positive pathogens, peptidoglycan *O*-acetyltransferase A (OatA). *PLoS Pathog.* **13,** e1006667 CrossRef Medline
30. Sychantha, D., and Clarke, A. J. (2018) Peptidoglycan modification by the catalytic domain of *Streptococcus pneumoniae* OatA follows a ping-pong bi-bi mechanism of action. *Biochemistry* **57,** 2394–2401 CrossRef Medline
31. Gmeiner, J., and Kroll, H.-P. (1981) Murein biosynthesis and *O*-acetylation of *N*-acetylmuramic acid during the cell-division cycle of *Proteus mirabilis*. *Eur. J. Biochem.* **117,** 171–177 Medline
32. Lear, A. L., and Perkins, H. R. (1986) *O*-Acetylation of peptidoglycan in *Neisseria gonorrhoeae*: investigation of lipid-linked intermediates and glycan chains newly incorporated into the cell wall. *J. Gen. Microbiol.* **132,** 2413–2420 Medline
33. Gmeiner, J., and Sarnow, E. (1987) Murein biosynthesis in synchronized cells of *Proteus mirabilis*: quantitative analysis of *O*-acetylated murein subunits and of chain terminators incorporated into the sacculus during the cell cycle. *Eur. J. Biochem.* **163,** 389–395 CrossRef Medline
34. Snowden, M. A., Perkins, H. R., Wyke, A. W., Hayes, M. V., and Ward, J. B. (1989) Cross-linking and *O*-acetylation of newly synthesized peptidoglycan in *Staphylococcus aureus* H. *J. Gen. Microbiol.* **135,** 3015–3022 Medline

35. Goldschmidt, L., Cooper, D. R., Derewenda, Z. S., and Eisenberg, D. (2007) Toward rational protein crystallization: a web server for the design of crystallizable protein variants. *Protein Sci.* **16,** 1569–1576 CrossRef Medline
36. Kell, L. F. (2015) Investigation of novel inhibitory compounds of *O*-acetyltransferase A (OatA) from *Staphylococcus aureus*, Ph.D. thesis, University of Guelph
37. Williams, A. H., Veyrier, F. J., Bonis, M., Michaud, Y., Raynal, B., Taha, M.-K., White, S. W., Haouz, A., and Boneca, I. G. (2014) Visualization of a substrate-induced productive conformation of the catalytic triad of the *Neisseria meningitidis* peptidoglycan *O*-acetylesterase reveals mechanistic conservation in SGNH esterase family members. *Acta Crystallogr. D* **70,** 2631–2639 CrossRef Medline
38. Moynihan, P. J., and Clarke, A. J. (2014) Mechanism of action of peptidoglycan *O*-acetyltransferase B involves a Ser-His-Asp catalytic triad. *Biochemistry* **53,** 6243–6251 CrossRef Medline
39. Brott, A. S., Jones, C. S., and Clarke, A. J. (2019) Development of a high throughput screen for the identification of inhibitors of peptidoglycan *O*-acetyltransferases, new potential antibacterial targets. *Antibiotics* **8,** E65 CrossRefMedline
40. Huynh, K., and Partch, C. L. (2015) Analysis of protein stability and ligand interactions by thermal shift assay. *Curr. Protoc. Protein Sci.* **79,** 28.9.1–28.9.14 CrossRefMedline
41. Otwinowski, Z., and Minor, W. (1997) Processing of X-ray diffraction data collected in oscillation mode. *Methods Enzymol.* **276,** 307–326 CrossRef Medline
42. Pape, T., and Schneider, T. R. (2004) HKL2MAP: a graphical user interface for macromolecular phasing with SHELX programs. *J. Appl. Crystallogr.* **37,** 843–844 CrossRef
43. Terwilliger, T. C. (2003) Automated main-chain model building by template matching and iterative fragment extension. *Acta Crystallogr. D* **59,** 38–44 CrossRef Medline
44. Terwilliger, T. C., Grosse-Kunstleve, R. W., Afonine, P. V., Moriarty, N. W., Zwart, P. H., Hung, L. W., Read, R. J., and Adams, P. D. (2008) Iterative model building, structure refinement and density modification with the *PHENIX AutoBuild* wizard. *Acta Crystallogr. D* **64,** 61–69 CrossRef Medline
45. Emsley, P., and Cowtan, K. (2004) COOT: model-building tools for molecular graphics. *Acta Crystallogr. D* **60,** 2126–2132 CrossRef Medline
46. Adams, P. D., Afonine, P. V., Bunkóczi, G., Chen, V. B., Echols, N., Headd, J. J., Hung, L.-W., Jain, S., Kapral, G. J., Grosse Kunstleve, R. W., McCoy, A. J., Moriarty, N. W., Oeffner, R. D., Read, R. J., Richardson, D. C., *et al.* (2011) The Phenix software for automated determination of macromolecular structures. *Methods.* **55,** 94–106 CrossRef Medline
47. Laemmli, U. K. (1970) Cleavage of structural proteins during the assembly of the head of bacteriophage T4. *Nature* **227,** 680–685 CrossRef Medline
48. Gerlt, J. A., Bouvier, J. T., Davidson, D. B., Imker, H. J., Sadkhin, B., Slater, D. R., and Whalen, K. L. (2015) Enzyme function initiative-enzyme similarity tool (EFI-EST): a web tool for generating protein sequence similarity networks. *Biochim. Biophys. Acta* **1854,** 1019–1037 CrossRef Medline